Chapter 22
LEAP-UCD-2017 Centrifuge Test Simulation at UNINA

Gianluca Fasano, Anna Chiaradonna, and Emilio Bilotta

Abstract Within the framework of the LEAP-UCD-2017 exercise, Type B simulations of centrifuge tests were conducted assuming a hypoplastic constitutive model for sand. Differently from the most common elastoplastic approach, the hypoplasticity does not decompose the strain rate into elastic and plastic parts and does not use explicitly the notions of the yield surface and plastic potential surface. The process followed to calibrate the constitutive model is presented in detail. The initial state of stresses in the analyzed mesh, the key parameters used in the dynamic simulation phase, and a comparison of the simulation with some experimental results are reported. All the simulations were performed using the model parameters calibrated by using the laboratory test data. Finally, a sensitivity analysis of computed displacement to soil density and ground motion intensity show the influence of such factors on the seismic soil response of liquefiable soils.

22.1 Introduction

The aim of this paper is to describe the process followed to calibrate the constitutive model, to obtain the initial state of stresses in the analyzed soil-deposit mesh, to properly document the key parameters used in the seismic simulation phase, and to briefly present a comparison of the simulations with some experimental results of the LEAP-UCD-2017 exercise.

The content of the paper focuses on the following features of the performed numerical simulations: (1) the constitutive model used in the simulations, which is quite different from the most popular approaches that are currently adopted for studying liquefaction; (2) the calibration process, which is described in details; and (3) a sensitivity study.

The set of model parameters were calibrated on both triaxial and simple shear tests. The same parameters are used in the simulation of centrifuge tests, which are

G. Fasano · A. Chiaradonna (✉) · E. Bilotta
Department of Civil, Architectural and Environmental Engineering, University of Napoli Federico II, Naples, Italy
e-mail: anna.chiaradonna@unina.it

B. Kutter et al. (eds.), *Model Tests and Numerical Simulations of Liquefaction and Lateral Spreading*, https://doi.org/10.1007/978-3-030-22818-7_22

carried out at the prototype scale. Type B simulations section includes a description of the discretization, the numerical integration scheme, and numerical damping used in the analysis.

A sensitivity study (simulations NS1–NS7, exploring the sensitivity of displacement to soil density and ground motion intensity) has been carried out with the same parameters and using the same numerical model adopted in the Type B simulations.

The paper is divided into four sections. After this Introduction, Sect. 22.2 covers the essential features of the constitutive model, the final model parameters, the calibration philosophy, and the assumptions used in the calibration process. It also presents a comparison between the predicted and experimental cyclic strength curves. Section 22.3 discusses the main features of the numerical analysis platform used in the simulation, the model geometry and the discretization details, the boundary conditions of the numerical model, the solution algorithm employed, and some assumptions used in the reported analyses. Section 22.4 presents a comparison between the results of the Type B predictions and those of one of the centrifuge experiments. Finally, Sect. 22.5 shows the main results of the sensitivity study to explore the role of the soil density and ground motion intensity on slope behavior.

22.2 Calibration Phase

22.2.1 Hypoplastic Constitutive Model

The constitutive model used in the simulation exercise is the hypoplastic model with intergranular strain concept (Von Wolffersdorff 1996; Niemunis and Herle 1997), implemented in the finite element code PLAXIS 2016 (Mašín 2010).

Hypoplasticity is a particular class of incrementally nonlinear constitutive models, developed specifically to predict the behavior of soils. The basic structure of the hypoplastic models has been developed during the 1990s at the University of Karlsruhe. In hypoplasticity, unlike in elastoplasticity, the strain rate is not decomposed into elastic and plastic parts, and the models do not use explicitly the notions of the yield surface and plastic potential surface. Still, the models are capable of predicting the important features of the soil behavior, such as the critical state, dependency of the peak strength on soil density, nonlinear behavior in the small and large strain range, and dependency of the soil stiffness on the loading direction.

Hypoplastic models can well represent deformations due to rearrangements of the grain skeleton. However, applications of the hypoplasticity to cyclic loading with small amplitudes revealed some shortcomings. In the basic hypoplastic model (Von Wolffersdorff 1996), the stiffness during loading and reloading is almost identical, which leads to an unrealistic large accumulation of deformation in cyclic loading. Therefore, for simulations of cyclic or seismic loading, it is necessary to enhance the model with an extension, considering an increased stiffness in a small strain range. Thus, the applied hypoplastic constitutive equation corresponds to the model by von

Wolffersdorff (1996) with the intergranular strain extension according to Niemunis and Herle (1997). In Plaxis, the constitutive model is integrated using explicit adaptive integration scheme with local sub-stepping (Mašín 2010).

The parameters of the hypoplastic model (Von Wolffersdorff 1996) are critical friction angle ϕ_c, critical void ratio at zero pressure e_{c0}, void ratio at the maximum density at zero pressure e_{d0}, maximum void ratio at zero pressure e_{i0}, granular hardness h_s, stiffness exponent n, and the exponents α and β. The parameter α affects the peak friction angle in dependence of relative density, while the soil stiffness is affected by the parameter β. Moreover, the intergranular strain extension (Niemunis and Herle 1997) requires further five parameters: R, m_R, m_T, β_r, and χ. The stiffness increase after a change in the loading direction of 180° and 90° is controlled by the parameters m_R and m_T, respectively, with the loading direction referring to the direction of the strain rate. If $m_R = 0$, the intergranular strain concept is switched off, and the problem is simulated using the basic hypoplastic model (Von Wolffersdorff 1996).

The reduction in the shear modulus with increasing shear strain is controlled by the parameters R, β_r, and χ.

Finally, in addition to the initial void ratio, e_0, further six state parameters may be specified, δ_{11}, δ_{22}, δ_{33}, δ_{12}, δ_{13}, δ_{23}, which are the initial values of the intergranular strain tensor $\delta = (\delta_{11}, \delta_{22}, \delta_{33}, 2\delta_{12}, 2\delta_{13}, 2\delta_{23})$. They describe the accumulation of permanent deformation. Their initial values have been set to zero. A more detailed description of the model can be found in the referenced publications.

Table 22.1 reports the input parameters used in the hypoplastic model, as listed in Plaxis 2016 (Brinkgreve et al. 2016). The model requires overall 21 input parameters.

Table 22.1 Input parameters of the hypoplastic model

ϕ_c [°]	Critical state friction angle
p_t [kPa]	Shift of mean stress due to cohesion
h_s [kPa]	Overall slope of compression curve
n	Curvature of compression curve
e_{d0}	Densest particle packing at zero mean stress
e_{c0}	Critical particle packing at zero mean stress
e_{i0}	Loosest particle packing at zero mean stress
α	Peak friction angle as function of relative density
β	Shear stiffness as function of relative density
m_R	Initial shear stiffness for initial and reverse condition
m_T	Stiffness upon neutral condition
R	Size elastic range
β_r	Rate stiffness degradation
χ	Rate stiffness degradation
SV: e_0	Initial void ratio
δ_{ij} $i, j = 1,2,3$	Initial value of the intergranular strain tensor

22.2.2 Model Calibration

The approach used in the calibration of the model parameters is hereafter explained. The calibration made use of the results of the provided cyclic triaxial stress-controlled tests and additional element test data (i.e., monotonic triaxial tests, simple shear tests).

Shear strength parameters are computed from the monotonic triaxial test data, available on the NEES Hub (https://nees.org/dataviewer/view/1064:ds/1189). Drained triaxial compression tests, carried out by Vasko (2015) on loose and dense specimens, were used to define the critical state line in the plane $q{:}p'$ and the constant volume friction angle, ϕ'_c. As well known, the evaluation of critical state conditions in triaxial tests is a very complex issue, being such a test intrinsically affected by a number of experimental limitations (localization, bulging, shear stresses on the rough porous stones, difference between local and external displacements, etc.). One of the best ways to evaluate the final state is therefore by looking to dilatancy trend at the end of the tests. Based on all the elaborations of the available experimental data and considering that the hypoplastic model assumes the critical state as an asymptotic state at infinite strains, in this case the best fit of this parameter is the following:

$$\phi_c = 32^{\circ} \tag{22.1}$$

The critical void ratio at zero mean stress, e_{c0}, has been assumed, by extrapolation of experimental values as

$$e_{c0} = 0.746 \tag{22.2}$$

Hence, the other two parameters representing the initial values at $p' = 0$ of maximum and minimum void ratios have been set equal to

$$e_{d0} = e_{min} \tag{22.3}$$

$$e_{i0=1.2} e_{c0} \tag{22.4}$$

The parameter α was computed as a function of the void ratios, e, e_c, e_d, related to the peak mean stress, according to the equation proposed by Herle and Gudehus (1999):

$$\alpha = \frac{\ln\left[6\dfrac{\left(2+\mathrm{K}_p\right)^2+\mathrm{a}^2\mathrm{K}_p\left(\mathrm{K}_p-1-\tan\nu_p\right)}{\mathrm{a}\left(2+\mathrm{K}_p\right)\left(5\mathrm{K}_p-2\right)\sqrt{4+2\left(1+\tan\nu_p\right)^2}}\right]}{\ln\left[\dfrac{\mathrm{e}-\mathrm{e}_d}{\mathrm{e}_c-\mathrm{e}_d}\right]} \tag{22.5}$$

where the peak ratios are function of the peak friction angle, ϕ_p,

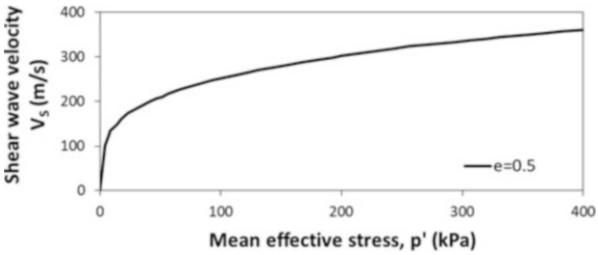

Fig. 22.1 Shear wave velocity measurements, V_S, vs. mean effective stress, p' during isotropic consolidation for Ottawa C-109 sand (modified after Robertson et al. 1995)

$$K_p = \frac{1 + \sin\phi_p}{1 - \sin\phi_p} \tag{22.6}$$

$$\tan\nu_p = 2\frac{K_p - 4 + 5AK_p{}^2 - 2AK_p}{(5K_p - 2)(1 + 2A)} - 1 \tag{22.7}$$

$$A = \frac{a^2}{(2 + K_p)^2}\left[1 - \frac{K_p(4 - K_p)}{4K_p - 2}\right] \tag{22.8}$$

while the parameter a is function of the critical friction angle, ϕ_c,

$$a = \frac{\sqrt{3}(3 - \sin\phi_c)}{2\sqrt{2}\sin\phi_c} \tag{22.9}$$

Finally, the parameter β was calibrated on the results of the available drained triaxial tests on dense specimens (Vasko 2015).

The parameters h_s and n were calibrated by interpolating the G_0:p' relationship proposed by Robertson et al. (1995) for dense Ottawa C-109 sand (Fig. 22.1) with the equation

$$G_0 = m_R \frac{h_s}{n}\left(\frac{3p}{h_s}\right)^{1-n}\left(\frac{e_{c0}}{e}\right)^{\beta} \times f_a \times f\langle K_0\rangle \tag{22.10}$$

where the constant of proportionality m_R has been set to 5 and

$$f_a = \left(\frac{e_{i0}}{e_{c0}}\right)^{\beta}\frac{1 + e_{i0}}{e_{i0}}\left[3 + a^2 - a\sqrt{3}\frac{e_{i0} - e_{d0}{}^{\alpha}}{e_{c0} - e_{d0}}\right]^{-1} \tag{22.11}$$

$$f\langle K_0\rangle = \frac{1}{2}\frac{\langle 1 + 2K^2\rangle + a^2\langle 1 - K\rangle}{1 + 2K^2} \tag{22.12}$$

with $K = \sigma_2/\sigma_1$, hence for isotropic stress $f(K) = 1.5$.

In Eq. (22.10), a shear wave velocity of 250 m/s was assumed for a reference value of mean stress, $p' = 100$ kPa (Fig. 22.1). Then, the stiffness at small strains, G_0 was computed as

$$G_0 = \rho V_S^2 \tag{22.13}$$

After that, the parameters h_s and n were calibrated to fit the G_0:p' relationship.

According to Mašín (2015), the parameter m_T was considered equal to a fraction of m_R:

$$m_T = 0.7 m_R \tag{22.14}$$

Figures 22.2a, b and 22.3a, b show the simulation of two monotonic triaxial tests (at 100 and 200 kPa of confining effective stress, respectively) on dense samples with dry density, $\rho_d = 1673$ kg/m^3 in the q:ε_a plane. The peak deviatoric values of both tests are well-predicted, while the simulated curves underestimate the stiffness and the dilatative behavior of the soil samples.

The implemented model requires also the definition of the parameter p_t, which is a shift of the mean stress due to cohesion. For the basic hypoplastic model, p_t is set equal to zero, but a nonzero value of p_t is needed to overcome problems with stress-free state (Mašín 2010).

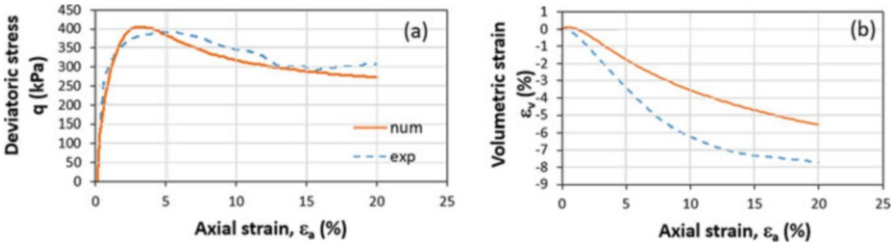

Fig. 22.2 Simulation of monotonic triaxial tests on dense Ottawa sand ($\rho_d = 1673$ kg/m^3) with p_0' equal to 100 kPa in the ε_a: q (**a**) and ε_a: ε_v (**b**) plane

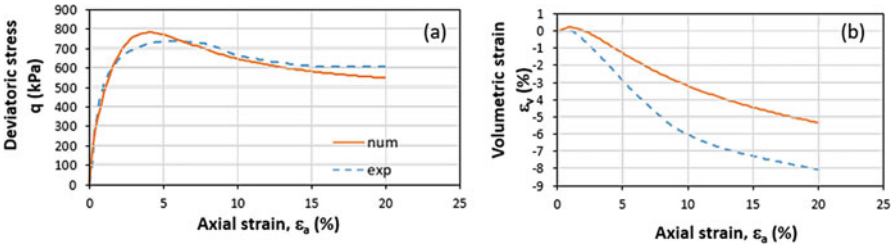

Fig. 22.3 Simulation of monotonic triaxial tests on dense Ottawa sand ($\rho_d = 1673$ kg/m^3) with p_0' equal to 200 kPa in the ε_a: q (**a**) and ε_a: ε_v (**b**) plane

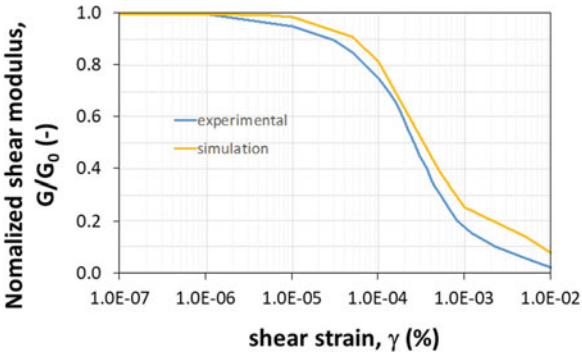

Fig. 22.4 Simulated shear modulus degradation curve vs. experimental curve for Ottawa sand 20–30 (modified after Alarcon-Guzman et al. 1989)

Table 22.2 Parameters of the hypoplastic model

ϕ_c [°]	p_t [kPa]	h_s [kPa]	n	e_{d0}	e_{c0}	e_{i0}	α	β	m_R	m_T	R_{max}	β_r	χ
32	1	304,836	0.51	0.507	0.746	0.896	0.18	1.5	5	3.5	0.0001	0.4	1

In order to identify the parameters R, β_r, and χ, simulations of strain-controlled cyclic shear tests were carried out, and the secant shear modulus G was evaluated from them. The numerical results have been compared with the experimental data for $(G/G_0, \gamma)$ reported in literature for Ottawa sand 20–30 (Alarcon-Guzman et al. 1989). The values of R and χ were assumed as $R = 0.0001$ and $\chi = 1.0$. Hence $\beta_r = 0.4$ was determined (Fig. 22.4).

The cyclic triaxial tests were simulated by using the "soil test" tool of Plaxis 2016 (Brinkgreve et al. 2016). The prescribed cyclic stress ratio, CSR_{CTX}, was imposed for a number of cycles, N, large enough to induce liquefaction. The model parameters that were finally obtained are summarized in Table 22.2. They were adopted for the simulation of the centrifuge tests.

22.2.3 Liquefaction Strength Curves

For each group of tests with the same void ratio, the relative density was defined as the mean value of the relative densities calculated by the different experimenters (see Table 22.3). For the sake of simplicity, the obtained mean values were rounded down. Table 22.3 shows that the available laboratory tests were performed on specimens of dense sand.

Figure 22.5 reports an example of the stress-strain and stress path curves simulated by the model for a cyclic stress-controlled test ($e_0 = 0.515$, $p'_0 = 100$ kPa, and

Table 22.3 Relative density according to the reported e_{min} and e_{max}

Tested by	Institute	e_{max}	e_{min}	$e_o = 0.515$	$e_o = 0.542$	$e_o = 0.585$
Eduardo Cerna	UC Davis	0.8375	0.5116	98.96%	90.67%	77.48%
Cooper Labs	UC Davis	0.7162	0.4977	92.08%	79.73%	60.05%
Wen-Yi Hung	NCU	0.7544	0.4599	81.29%	72.12%	57.52%
GeoComp (for RPI)	RPI	0.7403	0.479	86.22%	75.89%	59.43%
Yan-Guo (Eagle) ZHOU	Zhejiang University	0.7857	0.5003	94.85%	85.39%	70.32%
Ana Maria Parra Bastidas	UC Davis	0.791	0.4897	91.60%	82.64%	68.37%
Andrew Vasko	GWU	0.7389	0.4915	90.50%	79.59%	62.21%
Mean value				90%	80%	65%

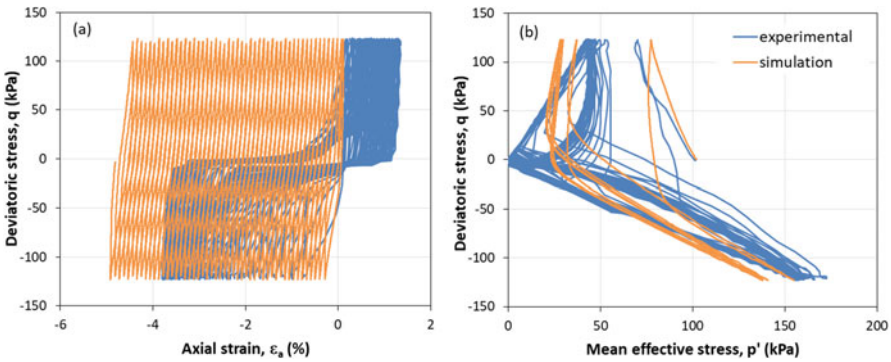

Fig. 22.5 Simulated stress-strain (**a**) and stress path (**b**) vs. experimental curve for a cyclic triaxial test with $e_0 = 0.515$, $p'_0 = 100$ kPa, and CSR = 0.6

CSR = 0.6) provided in El Ghoraiby et al. (2017) and compares them with the experimental data. The simulated stress-strain cycles are quite different from the experimental results, while the prediction of the stress path is satisfied especially during the extension phase of the test. Liquefaction has been assumed when a computed axial strain of 2.5% was achieved. It is worth noting that such a value is affected by ratcheting that is a common issue for many constitutive models among those implemented in commercial codes.

The liquefaction strength curves, obtained from the simulated cyclic stress-controlled triaxial tests, are plotted and compared with the experimental results (Fig. 22.6).

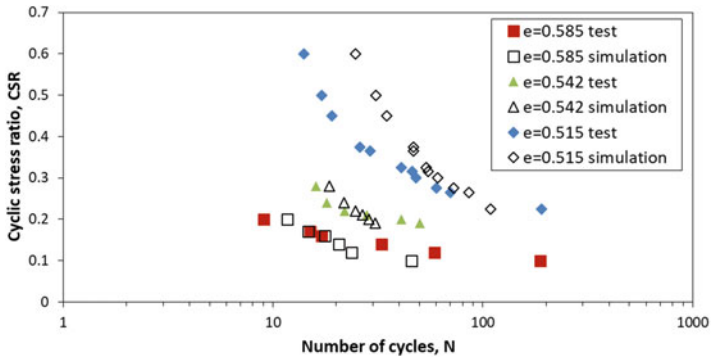

Fig. 22.6 Liquefaction strength curves obtained from experimental (El Ghoraiby et al. 2017, 2019) and simulated cyclic stress-controlled triaxial tests on Ottawa F65 Sand

22.3 Numerical Analysis Platform: Plaxis 2D

22.3.1 Analysis Platform

The simulations of the centrifuge tests have been carried out by using Plaxis 2D (Brinkgreve et al. 2016). This is a 2D commercial finite element method (FEM) code that includes several constitutive models. Many of them are available as user-defined model, such as the hypoplastic model with intergranular strain concept, implemented and made available in the platform by Mašín (2010).

The main reason to use Plaxis rather than other platforms is that, although not specifically oriented to solve boundary value problems in earthquake geotechnical engineering, this numerical code is quite well widespread in the community of geotechnical practitioners. Hence, it was interesting to check the possible benefit of a rigorous validation of numerical simulation procedures implemented in Plaxis through experimental data, in order to apply those procedures to a boundary value problem involving soil liquefaction.

Unfortunately, modelling the pore pressure dissipation during a dynamic analysis was not possible in Plaxis at the time when simulations were carried out. Therefore, pore pressure buildup needed to be calculated by imposing undrained conditions during shaking. This is obviously a limitation of the selected calculation method, since it affects the prediction of pore pressure buildup.

22.3.2 Model Geometry/Mesh and Boundary Conditions

Figure 22.7 shows the mesh density and the boundary conditions. The mesh consists of 428 15-noded triangular elements with an average size of 0.6 m. The nodes located

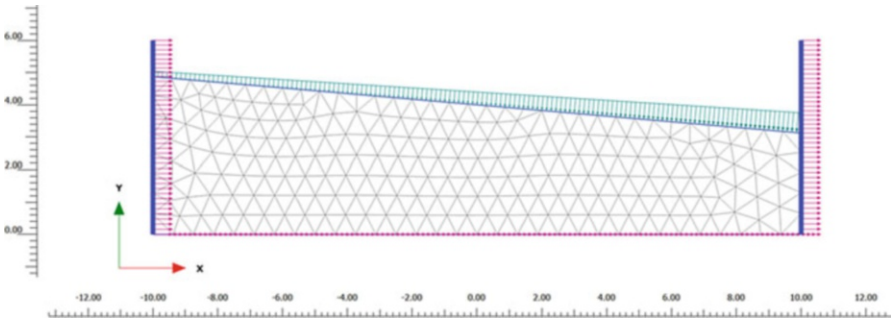

Fig. 22.7 Finite element model

at the base are fully constrained in *x*- and *y*-direction, while the nodes on the side walls are constrained laterally. The nodes on the ground surface allow full drainage.

22.3.3 Solution Algorithm and Assumptions

The Newmark time integration scheme is used in the simulations where the time step is constant and equal to the critical time step during the whole analysis. The proper critical time step for dynamic analyses is estimated in order to model accurately wave propagation and reduce error due to integration of time history functions. First, the material properties and the element size are taken into account to estimate the time step, and then the time step is adjusted based on the time history functions used in the calculation. During each calculation step, the Plaxis calculation kernel performs a series of iterations to reduce the out-of-balance errors in the solution. To terminate this iterative procedure when the errors are acceptable, it is necessary to establish the out-of-equilibrium errors at any stage during the iterative process automatically. Two separate error indicators are used for this purpose, based on the measure of either the global equilibrium error or the local error. The "global error" is related to the sum of the magnitudes of the out-of-balance nodal forces. The term "out-of-balance nodal forces" refers to the difference between the external loads and the forces that are in equilibrium with the current stresses. Such a difference is made nondimensional dividing it by the sum of the magnitudes of loads over all nodes of all elements. The "local error" is related to a norm of the difference between the equilibrium stress tensor and the constitutive stress tensor. It is made nondimensional dividing by the maximum value of the shear stress as defined by the failure criterion. The values of both indicators must be below a tolerated error set to 0.01 for the iterative procedure to terminate. In general, the solution procedure restricts the number of iterations that take place to 60, in order to ensure that computer time does not become too high.

A full Rayleigh damping formulation has been considered in the simulation, and the coefficients α_{RAY} and β_{RAY} are equal to 0.025 and 0.63×10^{-3}, respectively.

22.4 Type B Simulations

22.4.1 State of Stresses and Internal Variables of the Constitutive Model in the Pre-shaking Stage

All the centrifuge models are subjected to centrifugal accelerations that are increased from 1 g to a designated value during the spin-up process. The soil specimen is subjected to an increasing centrifugal acceleration that affects the state of stresses and the subsequent seismic response. The initialization of stresses and internal variables of the constitutive model after the centrifuge spin-up and just before the start of shaking was addressed in the simulation through a static analysis aimed at computing the initial effective stress state in the soil profile.

22.4.2 Results of the Dynamic Analysis

Relevant results of the simulations are hereafter discussed, while all the data of the numerical analysis can be found in the platform DesignSafe (www.designsafe-ci.org). As described in Kutter et al. (2019), the centrifuge model is monitored with accelerometers and pore pressure transducers as reported in Fig. 22.8.

Figure 22.9 shows the comparisons among simulated and predicted time histories of acceleration, pore pressure, and horizontal displacement at the surface for the

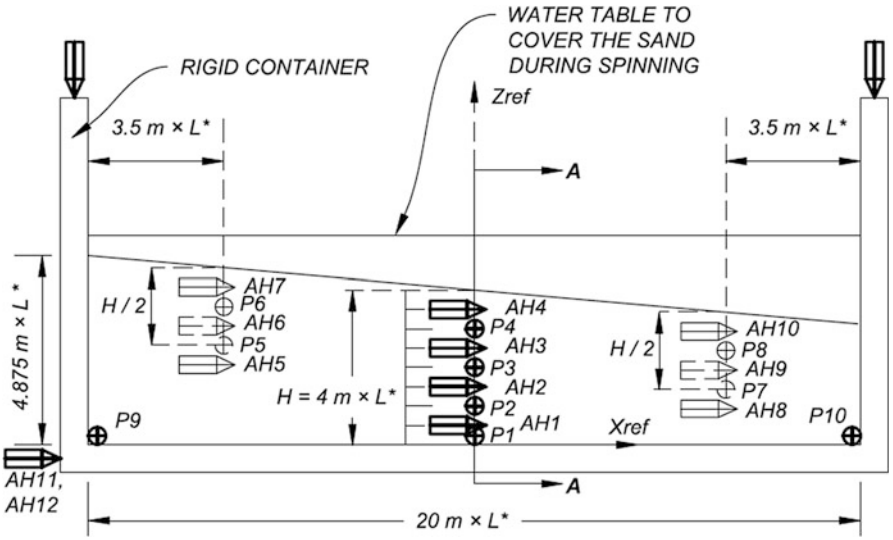

Fig. 22.8 Baseline schematic for centrifuge experiment for shaking parallel to the axis of the centrifuge (Kutter et al. 2019)

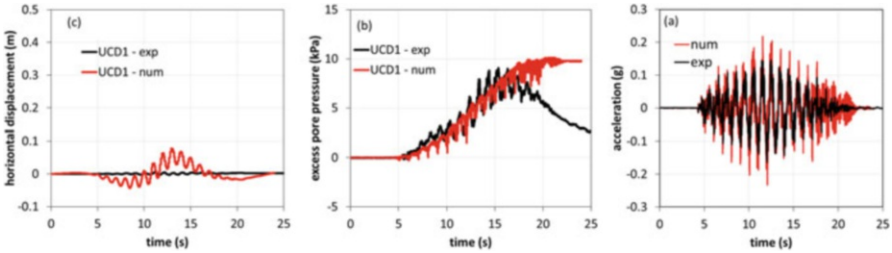

Fig. 22.9 Computed vs. measured acceleration time history of AH4 (**a**), pore pressure time history of P4 (**b**), and horizontal displacement at surface (**c**) in UCD 1 test

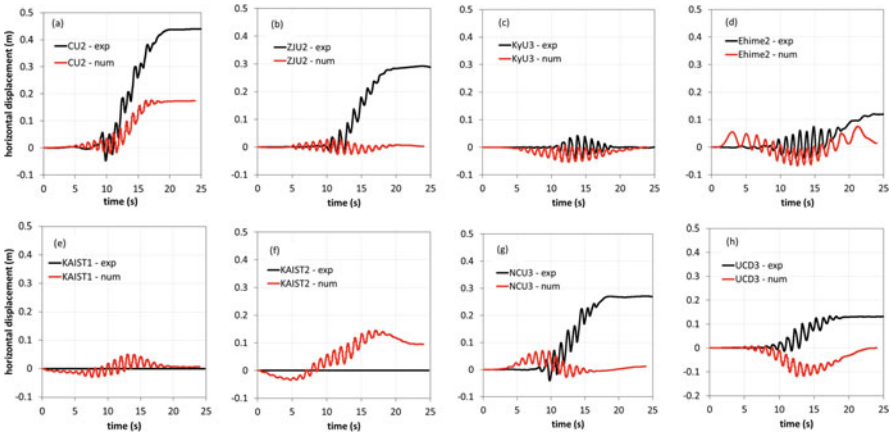

Fig. 22.10 Computed vs. measured horizontal displacement at surface in CU2 (**a**), ZJ2 (**b**), KyU3 (**c**), Ehime2 (**d**), KAIST1 (**e**), KAIST2 (**f**), NCU3 (**g**), and UCD3 (**h**) centrifuge test

UCD1 centrifuge test. A reasonable prediction of acceleration and pore pressure is provided by the numerical simulation, while simulated displacements strongly underestimate the experimental time history.

Since the horizontal displacements result to be the most critical aspect to be reproduced, the simulated displacements at the surface are compared to the experimental ones in all the other centrifuge tests (Fig. 22.10). The comparison shows that the amplitude of the simulated time histories is quite similar to the experimental one in centrifuge test KyU3 and Ehime 2 (Fig. 22.10c, d).

22.5 Sensitivity Analysis

The considered key input parameters of the sensitivity study are relative density and ground motion intensity, as described below. Table 22.4 shows the characteristics of each analysis.

Table 22.4 Characteristics of the analyses carried out for the sensitivity study

Simulation #	NS-1	NS-2	NS-3	NS-4	NS-5	NS-6	NS-7
Dry density (kg/m^3)	1651	1608	1683	1651	1651	1651	1651
Soil	Ottawa F65	Ottawa F65	Ottawa F65	Ottawa F65	Ottawa F65	Ottawa F65	Ottawa F65
D_r	65%	50%	75%	65%	65%	65%	65%
Input ground motion	Achieved RPI-1, Motion 1	Anticipated RPI-3 Motion 1	Achieved RPI-1, Motion 1	Achieved RPI-1, Motion 1 scaled up	Achieved RPI-1, Motion 1 scaled down	Achieved RPI-2 Motion 1	Achieved RPI-2 Motion 1 scaled up
PGA (g)	0.150	0.150	0.150	0.250	0.110	0.14	0.20
PGA—1 Hz comp. (g)	0.135	0.135	0.135	0.270	0.099	0.11	0.16
PGA—high freq (g)	0.021	0.021	0.021	0.035	0.015	0.08	0.11

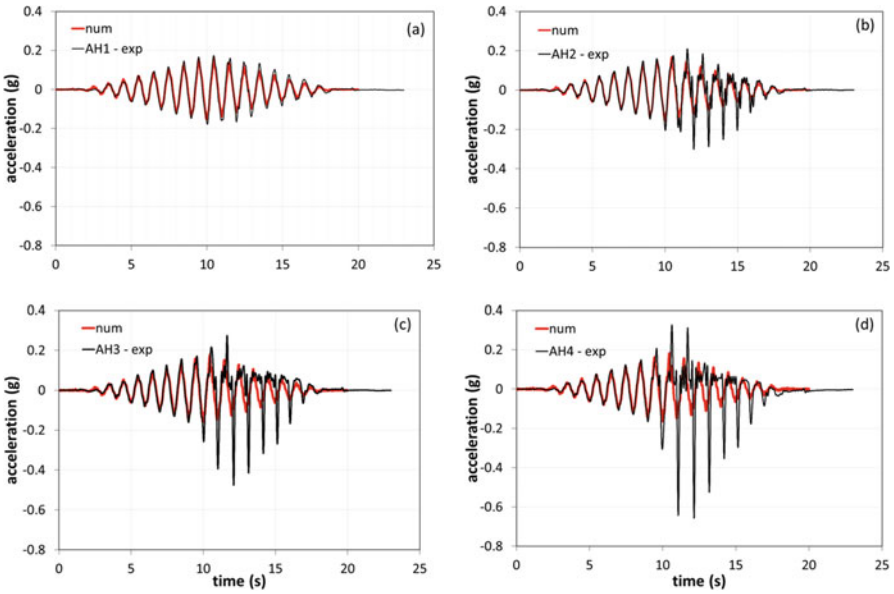

Fig. 22.11 Computed vs. measured acceleration time histories in AH1 (**a**), AH2 (**b**), AH3 (**c**), and AH4 (**d**)—RPI01 test

The sensitivity study incorporates Type C simulation of the RPI-1 test (simulation NS-1), Type B simulation of RPI-2 (NS-6) test, and an almost Type A simulation of RPI-3 (NS-2). NS-1 to NS-3 has been used to deduce the sensitivity of simulations to relative density. NS-1, NS-4, and NS-5 allowed deduction of the sensitivity of simulations to motion intensity. NS-6 and NS-7 allowed assessment of the influence of superimposed high frequencies on simulation results.

Figures 22.11, 22.12, and 22.13 report the comparison between computed and measured acceleration and pore pressure time histories related to the RPI01 centrifuge test. Experimental acceleration time histories are well-reproduced until liquefaction condition is attained; after that, the simulations lead to an underestimation of the observed trend. Underestimation is also related to the prediction of the pore pressure in the center of the model, while pore pressure closer to the boundaries of the laminar box are better simulated.

Table 22.5 summarizes the results of the analysis in terms of computed horizontal displacement at the middle point of the model surface. It must be noted that shaking was done imposing undrained conditions and a consolidation phase was run only after the end of the shaking; hence the analyses did not provide information about the duration of liquefaction after the end of shaking. In the following sections, the effects of relative density and motion intensity are shown.

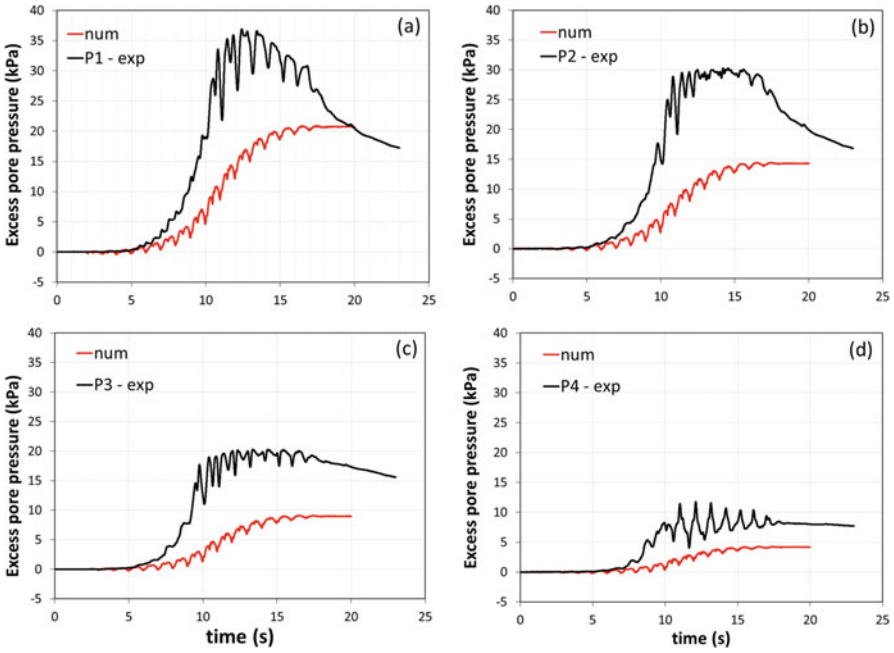

Fig. 22.12 Computed vs. measured EPP time histories in P1 (**a**), P2 (**b**), P3 (**c**), and P4 (**d**)—RPI01 test

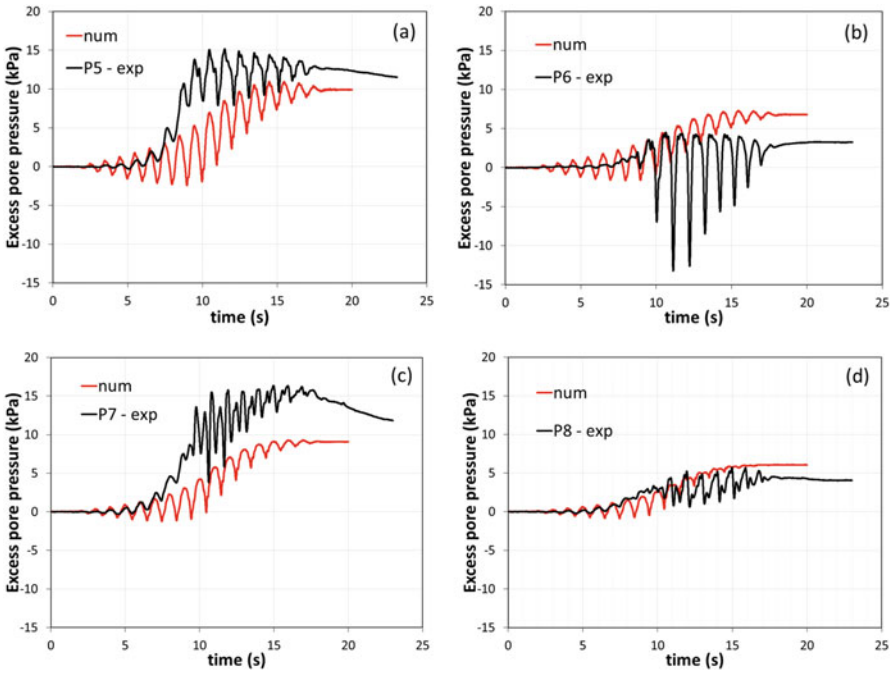

Fig. 22.13 Computed vs. measured EPP time histories in P5 (**a**), P6 (**b**), P7 (**c**), and P8 (**d**)—RPI01 test

Table 22.5 Main results of the sensitivity study

Simulation #	NS-1	NS-2	NS-3	NS-4	NS-5	NS-6	NS-7
X-displacement (m) at middle point on the model surface	7.1×10^{-4}	1.7×10^{-3}	5.8×10^{-4}	1.4×10^{-1}	4.4×10^{-4}	2.2×10^{-3}	2.5×10^{-1}

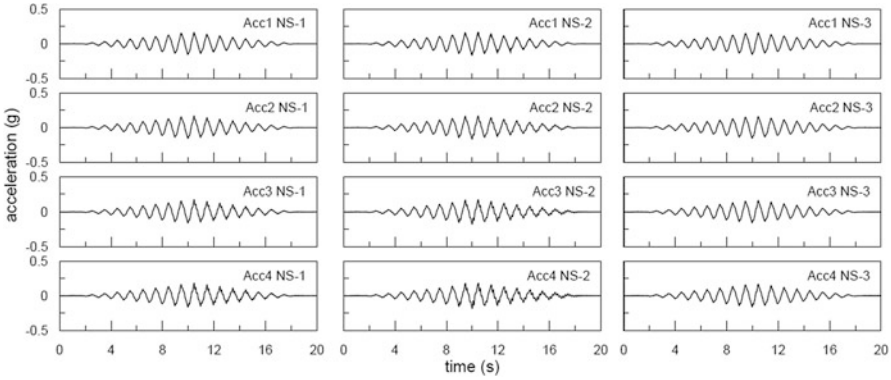

Fig. 22.14 Influence of relative density: simulated acceleration time histories

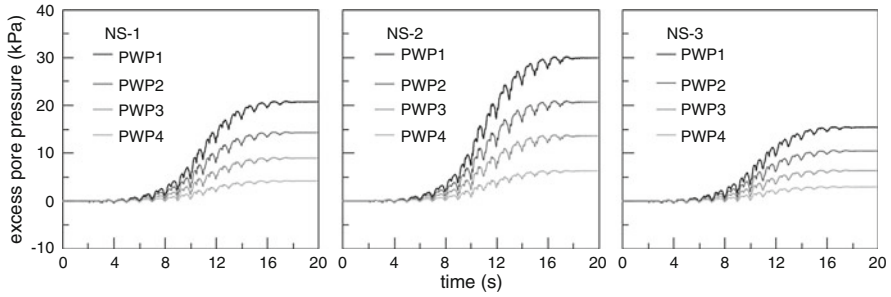

Fig. 22.15 Influence of relative density: simulated pore pressure time histories

22.5.1 Influence of Relative Density

With reference to the influence of relative density, three different analyses were carried out with a relative density of 65% (NS-1), 50% (NS-2), and 75% (NS-3), as reported in Fig. 22.14.

Small differences can be observed in the simulated acceleration time histories (Fig. 22.14), while higher pore pressure are generated for decreasing values of relative density (Fig. 22.15).

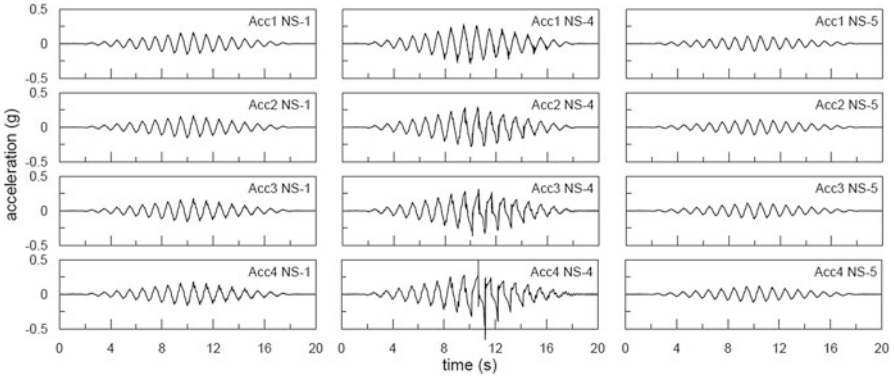

Fig. 22.16 Influence of motion intensity: simulated acceleration time histories

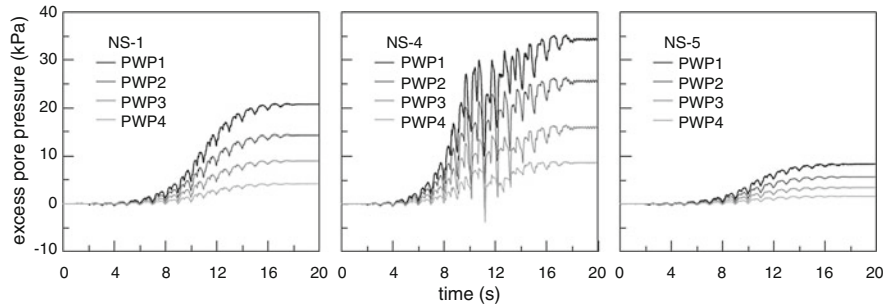

Fig. 22.17 Influence of motion intensity: simulated pore pressure time histories

22.5.2 Influence of Motion Intensity

With reference to the influence of input motion, three different analyses were carried out with a maximum acceleration of 0.15 g (NS-1), 0.25 g (NS-4), and 0.11 g (NS-5), as reported in Fig. 22.16. As expected, significant differences can be observed in the simulated acceleration time histories along the vertical profile (Fig. 22.16), while higher pore pressure are generated for increasing values of the maximum acceleration (Fig. 22.17).

22.6 Conclusion

This paper described the model calibration and numerical simulations of centrifuge test for LEAP-UCD-2017, carried out at the University of Napoli Federico II (Italy).

The adopted hypoplastic model allowed a relatively easy calibration of the model parameters compared to other advanced models. Cyclic resistance curves are well-

predicted although with some drawbacks on the shear strain histories, where "ratcheting" effects can be identified.

Modelling pore pressure dissipation during dynamic analysis was not possible in the version of Plaxis available at the time of simulations. Therefore, pore pressure buildup needed to be calculated by imposing undrained conditions during shaking. Nevertheless, in most cases, the buildup of excess pore pressure was reasonably captured. However, the magnitude of calculated horizontal displacements was in most cases unsatisfactory.

The sensitivity study highlighted the crucial role of relative density and the intensity of the applied input motion on the liquefaction behavior of the slope.

Acknowledgments The authors would like to thank the graduate students Giuseppe Colamarino, Giovanna Landolfo, and Gerardo Mascolo that carried out part of the simulations. Further appreciation goes to Prof Alessandro Flora and Prof Francesco Silvestri for their constructive comments and fruitful discussion. The Authors also wish to thank Prof David Masin for making available the Plaxis implementation of the sand hypoplasticity model used in the paper through the website www.soilmodels.com.

References

Alarcon-Guzman, A., Chameau, J. L., Leonards, G. A., & Frost, J. D. (1989). Shear modulus and cyclic undrained behavior of sands. *Soils and Foundations, 29*(4), 105–119.

Brinkgreve, R. B. J., Kumaeswamy, S., & Swolfs, W. M. (2016). *PLAXIS 2016 User's manual*. Retrieved from PLAXIS Website, https://www.plaxis.com/kb-tag/manuals/

El Ghoraiby, M. A., Park, H., & Manzari, M. T. (2017). *LEAP 2017: Soil characterization and element tests for Ottawa F65 sand*. Washington, DC: The George Washington University.

El Ghoraiby, M. A., Park, H., & Manzari, M. T. (2019). Physical and mechanical properties of Ottawa F65 sand. In B. Kutter et al. (Eds.), *Model tests and numerical simulations of liquefaction and lateral spreading: LEAP-UCD-2017*. New York: Springer.

Herle, I., & Gudehus, G. (1999). Determination of parameters of a hypoplastic constitutive model from properties of grain assemblies. *Mechanics of Cohesive-Frictional Materials, 4*, 461–486.

Kutter, B. L., Carey, T., Stone, N., Zheng, B.L., Gavras, A., Manzari, M., et al. (2019). LEAP-UCD-2017 comparison of centrifuge test results. In B. Kutter et al. (Eds.), *Model tests and numerical simulations of liquefaction and lateral spreading: LEAP-UCD-2017*. New York: Springer.

Mašín, D. (2010). *PLAXIS implementation of hypoplasticity*. Retrieved March 2010 from PLAXIS Website.

Mašín, D. (2015). *Hypoplasticity for Practical Applications*. PhD course on hypoplasticity at Zhejiang University, June 2015. Retrieved from http://web.natur.cuni.cz/uhigug/masin/hypocourse/download/Hypoplasticity-course-handouts-public.pdf

Niemunis, A., & Herle, I. (1997). Hypoplastic model for cohesionless soils with elastic strain range. *Mechanics of Cohesive-Frictional Materials, 2*, 279–299.

Robertson, P. K., Sasitharan, S., Cunning, J. C., & Sego, D. C. (1995). Shear-wave velocity to evaluate in-situ state of Ottawa sand. *Journal of Geotechnical Engineering, 121*, 262–273.

Vasko, A. (2015). *An investigation into the behavior of Ottawa sand through monotonic and cyclic shear tests*. Master Thesis, The George Washington University.

Von Wolffersdorff, P. A. (1996). A hypoplastic relation for granular materials with a predefined limit state surface. *Mechanics of Cohesive-Frictional Materials, 1*, 251–271.